The effect of self-aggregation on the determination of the kinetic and thermodynamic constants of the network of chemical reactions in 3-glucoside anthocyanins

ARTICLE *in* PHYTOCHEMISTRY · AUGUST 2012

Impact Factor: 2.55 · DOI: 10.1016/j.phytochem.2012.06.022 · Source: PubMed

7 AUTHORS, INCLUDING:

Ana Marta Diniz
New University of Lisbon
9 PUBLICATIONS **76** CITATIONS
SEE PROFILE

A. Jorge Parola
New University of Lisbon
119 PUBLICATIONS **1,826** CITATIONS
SEE PROFILE

João Carlos Lima
New University of Lisbon
143 PUBLICATIONS **2,217** CITATIONS
SEE PROFILE

F. Pina
New University of Lisbon
205 PUBLICATIONS **3,781** CITATIONS
SEE PROFILE

Phytochemistry 83 (2012) 125–135

Contents lists available at SciVerse ScienceDirect

Phytochemistry

journal homepage: www.elsevier.com/locate/phytochem

The effect of self-aggregation on the determination of the kinetic and thermodynamic constants of the network of chemical reactions in 3-glucoside anthocyanins

Yoann Leydet, Raquel Gavara, Vesselin Petrov, Ana M. Diniz, A. Jorge Parola, João C. Lima, Fernando Pina *

REQUIMTE, Departamento de Química, Faculdade de Ciências e Tecnologia, Universidade Nova de Lisboa, 2829-516 Monte de Caparica, Portugal

ARTICLE INFO

Article history:
Received 20 April 2012
Received in revised form 24 June 2012
Available online 18 August 2012

Keywords:
Anthocyanins
Aggregation
3-Glucosides
Protonation
Hydration
Tautomerization
Isomerization

ABSTRACT

The six most common 3-glucoside anthocyanins, pelargonidin-3-glucoside, peonidin-3-glucoside, delphinidin-3-glucoside, malvidin-3-glucoside, cyanidin-3-glucoside and petunidin-3-glucoside were studied in great detail by NMR, UV–vis absorption and stopped flow. For each anthocyanin, the thermodynamic and kinetic constants of the network of chemical reactions were calculated at different anthocyanin concentration, from 6×10^{-6} M up to 8×10^{-4} M; an increasing of the flavylium cation acidity constant to give quinoidal base and a decreasing of the flavylium cation hydration constant to give hemiketal were observed by increasing the anthocyanin concentration. These effects are attributed to the self-aggregation of the flavylium cation and quinoidal base, which is stronger in the last case. The UV–vis and ^{1}H NMR spectral variations resulting from the increasing of the anthocyanin concentration were discussed in terms of two aggregation models; monomer–dimer and isodesmic, the last one considering the formation of higher order aggregates possessing the same aggregation constant of the dimer. The self-aggregation constant of flavylium cation at pH = 1.0, calculated by both models increases by increasing the number of methoxy ($-OCH_3$) or hydroxy (–OH) substituents following the order: myrtillin (2 –OH), oenin (2 $-OCH_3$), 3-OGl-petunidin (1 –OH, 1 $-OCH_3$), kuromanin (1 –OH), 3-OGl-peonidin (1 $-OCH_3$) and callistephin (none). Evidence for flavylium aggregates possessing a shape between J and H was achieved, as well as for the formation of higher order aggregates.

1. Introduction

Anthocyanins are the ubiquitous colorants of most flowers and fruits and have been the subject of numerous studies not only to explain the phenomenon of the color in plants (Dangles et al., 1993; Goto and Kondo, 1991; Kondo et al., 1992, 2001; Mateus and Freitas, 2009; Yoshida et al., 1995, 2009) but also to exploit the potential of these compounds in practical applications, from food colorants (Brouillard, 1982; Castañeda-Ovando et al., 2009) to drugs with great benefits for the human health (Bagchi et al., 2000; Kalt et al., 2001). The research on anthocyanins and related compounds is a long story with more than one century, involving two Nobel prizes, Richard Willsttäter (1915) and Robert Robinson (1947) and thousands of contributions from an extensive scientific community. The first compound related to anthocyanins was reported by Bülow and Wagner (1901), who synthesized 4-methyl-7-hydroxyflavylium. However, only by the eighties of the 20th century a clear picture of the network of chemical reactions of anthocyanins was obtained, in particular after the works of Dubois and Brouillard (Brouillard and Lang, 1990; Brouillard et al., 1978; Brouillard and Delaporte, 1977) and McClelland (McClelland and McGall, 1982; McClelland and Gedge, 1980).

It is now firmly established that anthocyanins and related compounds are involved in a series of chemical reactions defining a network as shown in Scheme 1 for malvidin-3-glucoside (oenin) in moderately acidic solutions.

The flavylium cation, **AH$^+$**, is the predominant species in the equilibrium under sufficiently acidic conditions. When the pH is raised the flavylium cation is involved in two parallel reactions: (i) deprotonation to form the quinoidal base, **A**, (ii) hydration in position 2 to give the hemiketal **B2**, hereon referred as **B**. The proton transfer is faster than the hydration but in general at least some of the other species (**B**, **Cc**, **Ct**) are more stable than **A** at the equilibrium. Consequently, **A** can be formed as a kinetic product and later totally or partially disappears to yield the thermodynamic equilibrium. The key step of this process is the formation of **B** exclusively through the hydration of **AH$^+$**, in other words, **A** does not give directly **B**, unless in basic medium (Brouillard et al., 1978).

* Corresponding author.
E-mail address: fp@fct.unl.pt (F. Pina).

0031-9422/$ - see front matter © 2012 Elsevier Ltd. All rights reserved.
http://dx.doi.org/10.1016/j.phytochem.2012.06.022

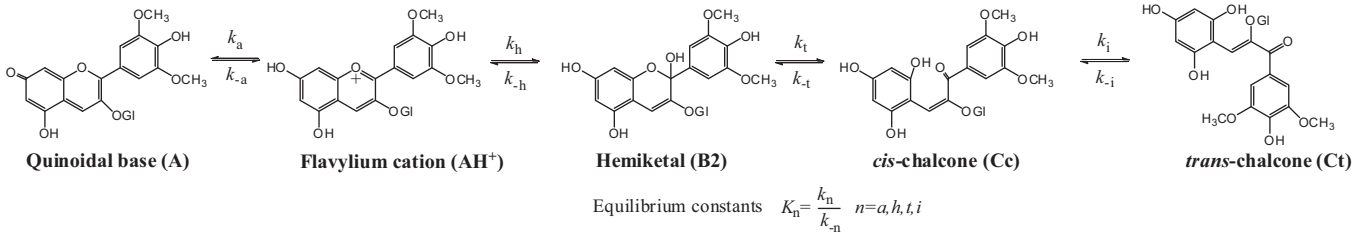

Scheme 1. Network of chemical reactions of malvidin-3-glucoside (oenin) in acidic medium.

The *cis*-chalcone (**Cc**) is formed from **B** by a tautomeric process and the *trans*-chalcone (**Ct**) via the isomerization of the former. The colored species are **AH$^+$** and **A**, responsible for red and blue colors, respectively.

Inspection of the thermodynamic and kinetic constants of anthocyanins published in literature evidences the existence of a great discrepancy between the values reported by different authors (Pina et al., 2012). The point is that these constants are dependent on the ionic strength, temperature, but more relevant, on the anthocyanin concentration. This is essentially due to self-association leading to the formation of aggregates, as previously evidenced by several techniques including UV–vis absorption spectroscopy, circular dichroism and NMR (Asen et al., 1972, 1975; Hoshino, 1991, 1992; Hoshino and Goto, 1990; Hoshino et al., 1980, 1981a,b, 1982; Houbiers et al., 1998). The self-association takes place with the flavylium cation as well as with the quinoidal base. Cross aggregation involving flavylium cation and *trans*-chalcone were also described for malvidin-3-glucoside (oenin) on the basis of the ^{1}H NMR data (Houbiers et al., 1998). The formation of co-pigments and self-aggregates has been claimed to make more difficult the hydration processes rendering the pigment more stable (Dangles et al., 1993). However, no detailed study of concentration dependence of the rate and equilibrium constants of the network of chemical reactions involving anthocyanins was reported. Here we present a detailed study of the effect of the anthocyanin concentration on the thermodynamic and kinetic constants of the network of chemical reactions taking place in the six most common 3-glucoside anthocyanins. We would like to answer in particular the following questions: (i) how significant are the differences in equilibrium constants usually correlated with substitution pattern without taking into account the self-aggregation effect, (ii) what is the effect of the self-aggregation in the determination of the rate and equilibrium constants of anthocyanins, (iii) what is the evidence for the formation of high order aggregates.

2. Experimental

Myrtillin chloride, oenin chloride, kuromanin chloride and callistephin chloride were purchased from Extrasynthèse; peonidin-3-glucoside chloride and petunidin-3-glucoside chloride were purchased from PhytoLab. All the reagents (>99%) were used without any further purification. The solutions were prepared in Millipore water. The pH of the solutions was adjusted by the addition of HCl, NaOH or 2.5×10^{-3} M citrate buffer and was measured on a Radiometer Copenhagen PHM240 pH/ion meter. In the case of NMR studies, no buffer was used and the pH was adjusted only with HCl and NaOH. In all measurements, the ionic strength was kept constant at 0.1 M by the addition of NaCl. The ^{1}H NMR spectra were run at 298 K, on a BrukerAvance III 400 machine operating at 400.13 MHz, in pure (non-deuterated) water to allow direct comparison of data obtained from NMR and UV–vis measurements, in defined concentration ranges. The water peak was suppressed using an excitation sculpting scheme (Shaka and Hwang, 1995) and 1,4-dioxane was used as an internal reference. UV/vis absorption spectra were recorded on Varian Cary 100 Bio and Varian Cary 5000 spectrophotometers. The stopped flow experiments were conducted in an Applied Photophysics SX20 stopped flow spectrometer provided with a PDA.1/UV photodiode array detector with a minimum scan time of 0.65 ms and a wavelength range of 200–735 nm.

3. Results and discussion

The thermodynamics and kinetics of the network of chemical reactions involving the six most common anthocyanin 3-monoglucosides were studied, Scheme 2. The same experimental procedure was used to characterize each of the chemical reaction networks to allow comparisons of the data under identical conditions.

In order to account for the influence of the anthocyanin concentration on the thermodynamic and kinetic constants, the respective determination was carried out at several concentrations in the range 6.0×10^{-6}–8×10^{-4} M. Due to the high molar absorption coefficients of the flavylium cations and the quinoidal bases, diluted and moderately concentrated solutions were studied by UV–vis spectroscopy, using an optical path of 10 and 2 mm, respectively, while concentrated solutions, up to the solubility limit, were studied by ^{1}H NMR. In a second step the aggregation of species was analyzed by means of two different models.

From Scheme 1, the following set of equations account for the reactions taking place in the system:

$$\mathbf{AH}^+ + H_2O \leftrightharpoons \mathbf{A} + H_3O^+ \quad K_a \tag{1}$$

$$\mathbf{AH}^+ + 2H_2O \leftrightharpoons \mathbf{B} + H_3O^+ \quad K_h \tag{2}$$

$$\mathbf{B} \leftrightharpoons \mathbf{Cc} \quad K_t \tag{3}$$

$$\mathbf{Cc} \leftrightharpoons \mathbf{Ct} \quad K_i \tag{4}$$

The analysis of the thermodynamic equilibria becomes easier if Eq. (5) is considered. Eq. (5) is equivalent to a single acid–base equilibrium between flavylium cation and a conjugate base, **CB**, defined as the sum of the concentrations of the other species in the network, [**CB**] = [**A**] + [**B**] + [**Cc**] + [**Ct**] (Brouillard and Lang, 1990; Brouillard et al., 1978; Brouillard and Delaporte, 1977; Pina, 1998; Pina et al., 2012).

$$\mathbf{AH}^+ + H_2O \leftrightharpoons \mathbf{CB} + H_3O^+ \quad K'_a = K_a + K_h + K_hK_t + K_hK_tK_i \tag{5}$$

When a relatively high *cis*–*trans* isomerization barrier is present it is very useful to define a pseudo-equilibrium attained before formation of significant amounts of **Ct**.

$$\mathbf{AH}^+ + H_2O \leftrightharpoons \mathbf{CB}^\wedge + H_3O^+ \quad K^\wedge_a = K_a + K_h + K_hK_t \tag{6}$$

$$[\mathbf{CB}^\wedge] = [\mathbf{A}] + [\mathbf{B}] + [\mathbf{Cc}]$$

From the set of Eqs. (1)–(5) it is easy to obtain the pH dependent mole fraction distribution of the network species.

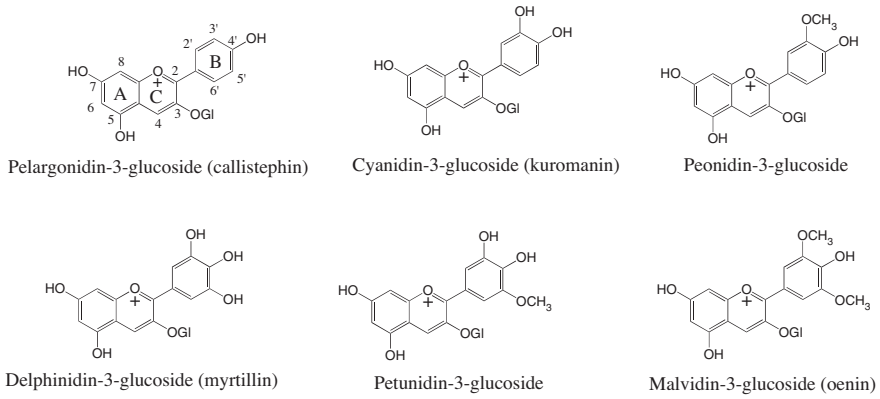

Scheme 2. Structures of the six most common 3-glucoside anthocyanins.

$$\chi_{AH^+} = \frac{[H^+]}{[H^+] + K'_a}; \quad \chi_A = \frac{K_a}{[H^+] + K'_a}; \quad \chi_B = \frac{K_h}{[H^+] + K'_a};$$
$$\chi_{Cc} = \frac{K_h K_t}{[H^+] + K'_a}; \quad \chi_{Ct} = \frac{K_h K_t K_i}{[H^+] + K'_a} \tag{7}$$

In the UV–vis studies, the following step by step approach was used at each concentration to calculate the rate and equilibrium constants of 3-glucoside anthocyanins, Scheme 3.

The experimental results are presented in detail for delphinidin-3-glucoside (myrtillin) while equivalent data for the other five anthocyanins are reported in Supporting information.

Determination of the myrtillin (2.0×10^{-5} M) pK'_a by UV–vis absorption was carried out from the pH dependence of the absorption spectra of equilibrated solutions. The decreasing of the absorbance of the flavylium cation was fitted for a single acid–base equilibrium according to Eq. (5), Fig. 1A (step 1 of Scheme 3).

The acid–base constant K_a was calculated by collecting the absorption spectra immediately after a pH jump from stock solutions of the flavylium cation at pH = 1 to higher pH values, see Fig. 1B for pH = 5.6. If the final pH is sufficiently high to consider complete conversion of the flavylium cation into the quinoidal base at $t = 0$, and a wavelength where only **A** absorbs is selected, the ratio between the final and the initial absorbances is equal to the mole fraction distribution of the quinoidal base at equilibrium, K_a/K'_a (Eq. (7) when $[H^+]$ tends to zero), see inset of Fig. 1B, with pK_a = 3.8, (step 2 in Scheme 3, Pina, 1998). In the context of this work direct pH jumps are those carried out from the flavylium cation equilibrated at very low pH to higher pH values, and reverse pH jumps those from equilibrated solutions at moderately acidic medium to lower pH values. Reverse pH jumps carried out in equilibrated solutions of myrtillin 2×10^{-5} M at pH = 4.5 back to pH = 1.4 and 1.0 were monitored by stopped flow, Fig. 2. The recovery of the flavylium cation absorption takes place in three steps, as reported in Fig. 2B: (i) **A** is transformed into **AH$^+$** during the mixing time of the stopped flow; (ii) the first part of the growth in absorption corresponds to the conversion of **B** into **AH$^+$**, k_{obs1}; (iii) the second part of the absorption increase is due to the small amount of **Cc** at the equilibrium that gives more flavylium cation through **B**, k_{obs2}. The system reaches the (final) equilibrium through a much slower process kinetically controlled by the *cis–trans* isomerization (not shown). The bi-exponential growth (steps ii and iii) takes place with rate constants $k_{obs1} = 1.2\ s^{-1}$ and $k_{obs2} = 0.3\ s^{-1}$ for a final pH = 1.4 and $k_{obs1} = 3.2\ s^{-1}$ and $k_{obs2} = 0.5\ s^{-1}$ for a final pH = 1.0. From the ratio of the pre-exponential factors of bi-exponential fitting the equilibrium constant $K_t = 0.06$ is calculated, Fig. 2B (step 3 of Scheme 3).

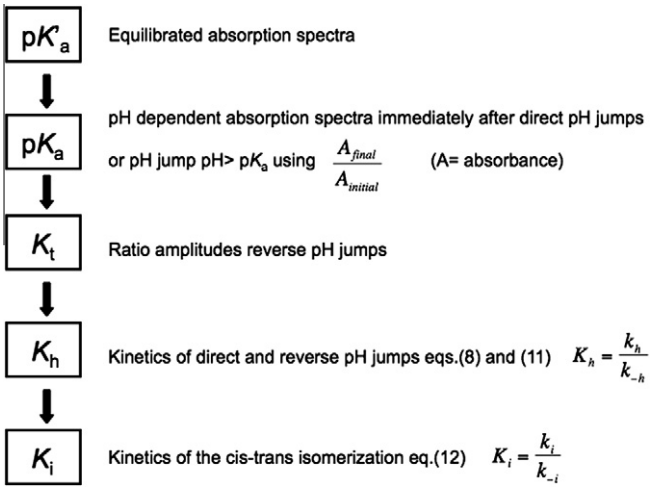

Scheme 3. Step by step procedure used to obtain the rate and equilibrium constants of anthocyanin-3-glucoside reaction networks.

The observed rate constants from reverse pH jumps correlate with the kinetic rate constants of the system through Eqs. (8) and (9). The disappearance of **B** is faster than its formation from **Cc** and the hydration follows Eq. (8) while the tautomerization follows Eq. (9).

$$k_{obs1} = \frac{[H^+]}{[H^+] + K_a} k_h + k_{-h}[H^+] \tag{8}$$

$$k_{obs2} = k_{-t} \tag{9}$$

The rate constant $k_{obs2} = 0.5\ s^{-1}$, at pH = 1.0, is assigned to k_{-t} because **B** does not accumulate. As a consequence, k_t must be calculated from the equilibrium constant K_t, and k_{-t}, leading to $k_t = 0.03\ s^{-1}$ at this pH, see Scheme 1. However, the errors of both constants are high due to the small amount of **Cc** present at the equilibrium.

In the case of direct pH jumps, the well separated timescales of the kinetic processes in anthocyanins, lead to three observed rate constants, k_{obs3}, k_{obs4} and k_{obs5}, that relate with the kinetic rate constants through Eqs. (10)–(12) (Pina et al., 2012).

$$k_{obs3} = k_a + k_{-a}[H^+] \tag{10}$$

$$k_{obs4} = \frac{[H^+]}{[H^+] + K_a} k_h + \frac{1}{1 + K_t} k_{-h}[H^+] \tag{11}$$

$$k_{obs5} = \frac{K_h K_t}{[H^+] + K_a + (1 + K_t) K_h} k_i + k_{-i} \tag{12}$$

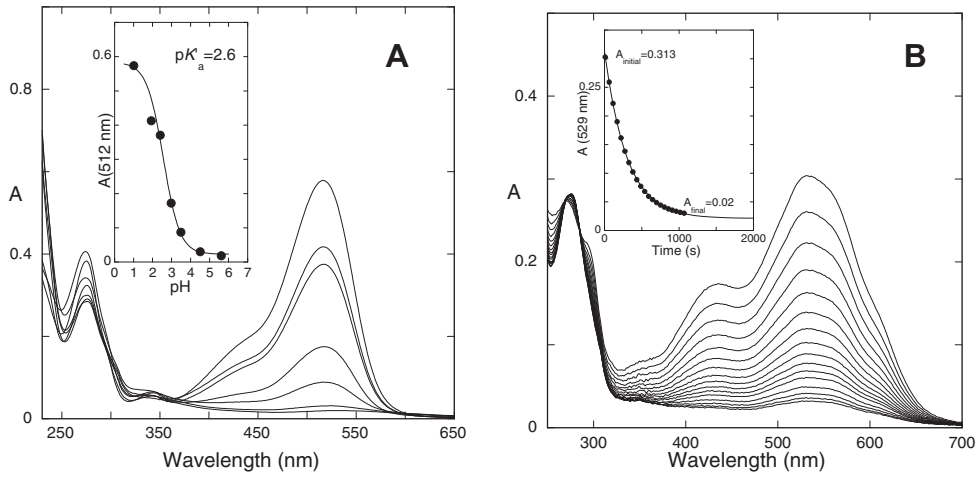

Fig. 1. (A) Absorption spectra of equilibrated solutions of myrtillin as a function of pH, 2.0×10^{-5} M; inset – determination of pK'_a using the absorbance at 512 nm. (B) Spectral variations of myrtillin 2.0×10^{-5} M upon a pH jump from pH = 1.0 to pH = 5.6; inset – variation of the absorbance at 529 nm, $pK_a = 3.8$.

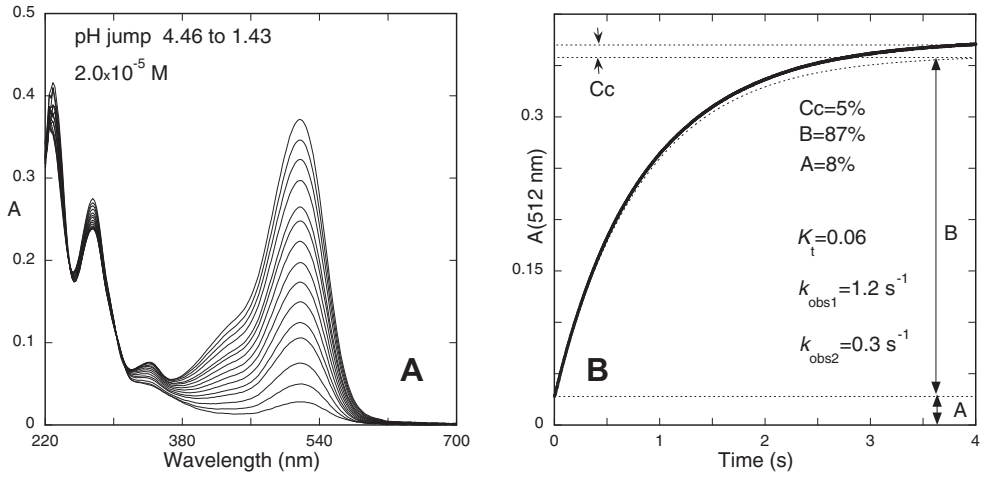

Fig. 2. (A) Spectral variations upon a reverse pH jump from an equilibrated solution of myrtillin 2×10^{-5} M at pH = 4.5 to pH = 1.4; (B) respective kinetic trace at 512 nm. Identical reverse pH jump to 1.0 leads to identical percentages of **A**, **B** and **Cc** and the following rate constants: $k_{obs1} = 3.2\ s^{-1}$ and $k_{obs2} = 0.5\ s^{-1}$.

Eq. (10) accounts for the deprotonation of the flavylium cation to give the quinoidal base, Eq. (11) regards the formation of the pseudo-equilibrium involving all the species of the network except *trans*-chalcone, and finally the system reaches the final equilibrium through Eq. (12). It is worth of note the fact that Eqs. (8) and (11) are similar and should be identical within experimental error if K_t is small, which is the case of anthocyanins.

A series of direct pH jumps of myrtillin 2.0×10^{-5} M at pH = 1.0 to higher pH values was carried out, Fig. 3.

The absorption immediately after the pH jump is a mixture of the flavylium cation and quinoidal base absorptions, due to the very fast protonation equilibrium, and k_{obs3} cannot be measured in the time scale of the experiment. At sufficiently high final pH values ($pH \geqslant pK_a + 2$), only the base is present at zero time. The subsequent disappearance of **A** takes place by two consecutive steps, both following first order kinetic laws, with rate constants $2.6 \times 10^{-3}\ s^{-1}$ and $2.4 \times 10^{-4}\ s^{-1}$ at pH = 5.6, Fig. 3A. The faster process corresponds to the formation of a pseudo-equilibrium involving **A** and **B** and **Cc**. The slower step is related to the formation of *trans*-chalcone from this pseudo-equilibrium. The *cis–trans* isomerization is much slower and while unequivocally observed, the absorbance variations are very small due to the low mole fraction of **Ct** at the equilibrium. The variation of the fast process as a function of pH is represented in Fig. 3B, joining results from both direct, k_{obs4}, and reverse, k_{obs1}, pH jumps.

The fitting of the data was achieved by means of Eq. (11), leading to $k_h = 0.09\ s^{-1}$ and $k_{-h} = 32\ M^{-1}\ s^{-1}$ (using $pK_a = 3.8$ and the above calculated value of $K_t = 0.06$), which allows to obtain $K_h = 2.8 \times 10^{-3}\ M^{-1}$ (step 4 in Scheme 3). Fitting with Eq. (8) leads to the same values of k_h and k_{-h}, within the experimental error. This experimental procedure was extended to the other five anthocyanins, see Supporting information, and Table 1.

The calculation of k_i and k_{-i} (step 5 in Scheme 3) presents a relatively high error because the concentration of **Ct** at the equilibrium is very small for all of the anthocyanins studied, and for this reason these constants were not included in Table 1.

3.1. Concentration effects on the thermodynamic and kinetic constants

NMR is a powerful technique to study the network of chemical reactions of anthocyanins at relatively high concentrations. The time needed to run an NMR spectrum is too long to allow the use of this technique to study fast reactions. However it is a powerful tool to study the equilibrium or to follow the kinetics of the slower processes. Here we decided to work in H_2O (non-deuterated water), avoiding corrections due to the deuterium isotopic effect,

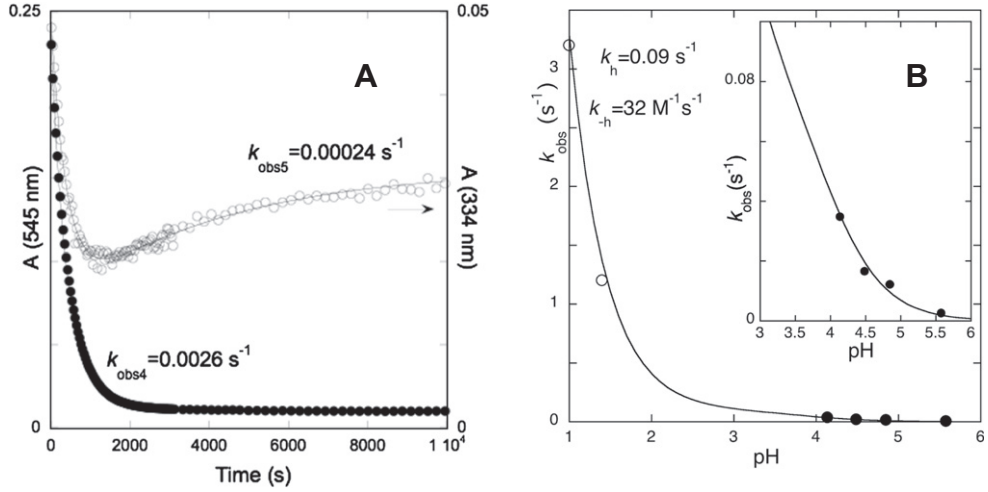

Fig. 3. (A) Changes in absorbance at 545 nm (closed circles) and 334 nm (open circles) of myrtillin 2.0×10^{-5} M after a pH jump from 1 to 5.6; (B) pH dependence of k_{obs4} (●) and k_{obs1} (○), fitted by means of Eq. (11); Fitting with Eq. (8) is coincident due to the low value of K_t; inset – magnification of the higher pH region.

Table 1
Data from UV–vis absorption, anthocyanin concentration 2.0×10^{-5} M.

Anthocyanin	pK'_a	pK_a	K_t[a]	K_h[a]	k_t (s^{-1})[a]	k_{-t} (s^{-1})[a]	k_h (s^{-1})[a]	K_{-h} (M^{-1} s^{-1})[a]
Myrtillin	2.6 ± 0.1	3.8 ± 0.1	0.06	2.8×10^{-3} M^{-1}	0.03[b]	0.5[b]	0.09	32
Oenin	2.3 ± 0.1	3.8 ± 0.1	0.12	3.4×10^{-3} M^{-1}	0.06[c]	0.5[c]	0.12	35
Petunidin	2.4 ± 0.1	3.7 ± 0.1	0.13	3.3×10^{-3} M^{-1}	0.08[c]	0.6[c]	0.10	30
Kuromanin	2.5 ± 0.1	3.8 ± 0.1	0.12	3.1×10^{-3} M^{-1}	0.07[c]	0.6[c]	0.11	35
Peonidin	2.4 ± 0.1	3.6 ± 0.1	0.26	4.9×10^{-3} M^{-1}	0.14[b]	0.5[b]	0.19	39
Callistephin	2.7 ± 0.1	3.9 ± 0.1	0.13	1.8×10^{-3} M^{-1}	0.11[c]	0.8[c]	0.12	67

[a] Estimated error ~20%.
[b] At pH = 1.0.
[c] At pH = 1.1.

to allow direct comparison of ^{1}H NMR and UV–vis data in the concentration regions where both techniques can be used (Glasoe and Long, 1960; Popov et al., 2006).

The identification of the ^{1}H NMR peaks for each component of the network (Fig. 4) can be accomplished following some simple observations: (i) the species **A** is in fast equilibrium with **AH$^+$** and conversion of **AH$^+$** into **A** by increasing pH is reflected in the chemical shift of the respective peaks to high field (Figueiredo et al., 1994); (ii) **B** is easily identified not only because it is the major species at higher pH values but also by the existence of twin peaks related to the presence of epimers (due to the appearance of the uncontrolled stereocenter C2 after the hydration); (iii) the chalcones usually appear in low concentrations but **Ct** can be easily identified due to its formation from the isomerization of **Cc**, which in anthocyanins is the slowest process. This last situation is well illustrated in Fig. 4B, where the growing of the **Ct** peaks is clearly observed. It is worth of note the fact that after 17 min the equilibrium between all the species of the network except **Ct** is already achieved and thus Fig. 4B only accounts for the process controlled by the *cis–trans* isomerization leading to the appearance of **Ct**.

Once the ^{1}H NMR peaks have been assigned it is possible to calculate the mole fraction distribution of each species of the network at the equilibrium, for different total concentration, Fig. 5.

Table 2 summarizes the equilibrium constants resulting from the fitting of the mole fractions obtained by ^{1}H NMR, for all the anthocyanins at two different concentrations, except for 3-OGl-peonidin

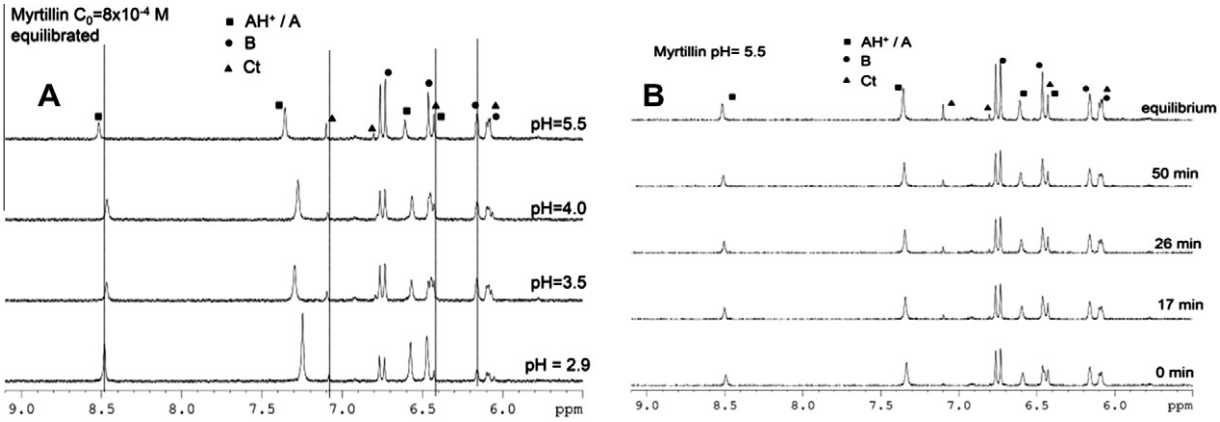

Fig. 4. (A) ^{1}H NMR spectra of myrtillin 8×10^{-4} M equilibrated at several pH values; (B) kinetics of the conversion of myrtillin 8×10^{-4} M, upon a pH jump from equilibrated solutions at pH = 1.0 to pH = 5.5, followed by ^{1}H NMR. Final equilibrium was achieved for $\chi_{AH^+/A} = 0.37$; $\chi_B = 0.56$; $\chi_{Ct} = 0.07$.

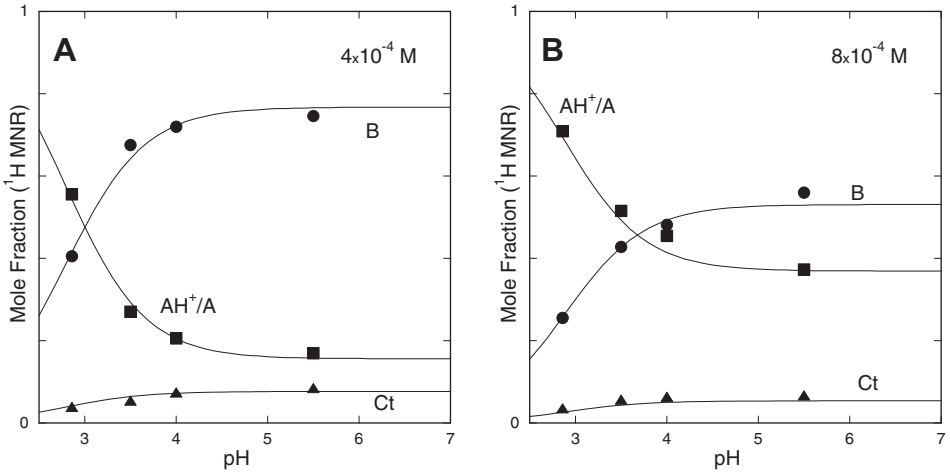

Fig. 5. Mole fraction distribution of **AH⁺/A** (■), **B** (●) and **Ct** (▲) as a function of pH. (A) [myrtillin] = 0.0004 M; fitting achieved $pK'_a = 2.8$, $pK_a = 3.6$, $K_h = 1.25 \times 10^{-3}\ M^{-1}$ and $K_hK_tK_i = 1.25 \times 10^{-4}\ M^{-1}$ using the mol fractions in Eq. (7). (B) [myrtillin] = 0.0008 M; fitting achieved with $pK'_a = 2.9$, $pK_a = 3.3$; $K_h = 6.9 \times 10^{-4}\ M^{-1}$; $K_hK_tK_i = 7.0 \times 10^{-5}\ M^{-1}$. The constants are apparent constants which include aggregation effects (see below).

Table 2
Observed apparent equilibrium constants obtained from the fitting of the ^{1}H NMR peaks area as a function of pH.

Anthocyanin	C_0 (M)	pK'_a	pK_a	K_h (M^{-1})	$K_hK_tK_i$ (M^{-1})
Myrtillin	4.0×10^{-4}	2.8 ± 0.1	3.6 ± 0.1	1.0×10^{-3}	1.25×10^{-4}
	8.0×10^{-4}	2.9 ± 0.1	3.3 ± 0.1	6.9×10^{-4}	7.0×10^{-5}
Oenin	4.0×10^{-4}	2.6 ± 0.1	3.4 ± 0.1	1.6×10^{-3}	2.9×10^{-4}
	8.0×10^{-4}	2.8 ± 0.1	3.3 ± 0.1	8.7×10^{-4}	1.4×10^{-4}
3-OGl-Petunidin	4.0×10^{-4}	2.7 ± 0.1	3.6 ± 0.1	1.6×10^{-3}*	3.5×10^{-4}
	8.0×10^{-4}	2.9 ± 0.1	3.6 ± 0.1	8.1×10^{-4}	1.5×10^{-4}
Kuromanin	4.0×10^{-4}	2.9 ± 0.1	3.5 ± 0.1	9.5×10^{-4}**	7.9×10^{-5}
	8.0×10^{-4}	3.2 ± 0.1	3.6 ± 0.1	4.2×10^{-4}	6.2×10^{-5}
Callistephin	4.0×10^{-4}	2.8 ± 0.1	3.5 ± 0.1	1.0×10^{-3}	1.8×10^{-4}
	8.0×10^{-4}	2.8 ± 0.1	3.3 ± 0.1	8.9×10^{-4}	1.4×10^{-5}

Estimated error 10%.
* 8.9×10^{-4} M by UV–vis.
** 1.3×10^{-4} M by UV–vis.

which is not soluble enough at the highest pH values. In Supporting information, ^{1}H NMR data and mole fractions for the other anthocyanins are shown.

Representation of K'_a, K_a and K_h obtained from ^{1}H NMR and from UV–vis as a function of myrtillin concentration (Fig. 6) illustrates the problem reported in the introduction: there is a clear dependence of the equilibrium constants on the anthocyanin concentration. An identical pattern was observed for the other anthocyanins, see Supporting information (in the case of peodinin its low solubility at moderately acidic pH values prevented determination for higher concentrations).

Extrapolation of the anthocyanin concentration to zero gives the equilibrium constants in the absence of self-aggregation and thus the data reported for the concentration 2×10^{-5} M can be considered a good approximation for the intrinsic behavior of the anthocyanins. The equilibrium constants at higher concentrations are apparent constants that reflect the effect of the aggregation.

As shown in Fig. 6, the observed pK'_a increases with increasing myrtillin concentration corresponding to a lower apparent reactivity of the flavylium cation at higher concentrations. The concentration dependence of K_a and K_h can in principle be explained on the basis of the known self-aggregation of both **AH⁺** and **A**, see Scheme 4. Aggregation of **A** increases acidity, while aggregation of **AH⁺** disfavors hydration. Moreover, the lower pK_a values for higher concentrations of the anthocyanin suggest stronger self-association for **A** than for **AH⁺**, which is expected as no positive charge repulsion occurs with **A** which additionally has a planar

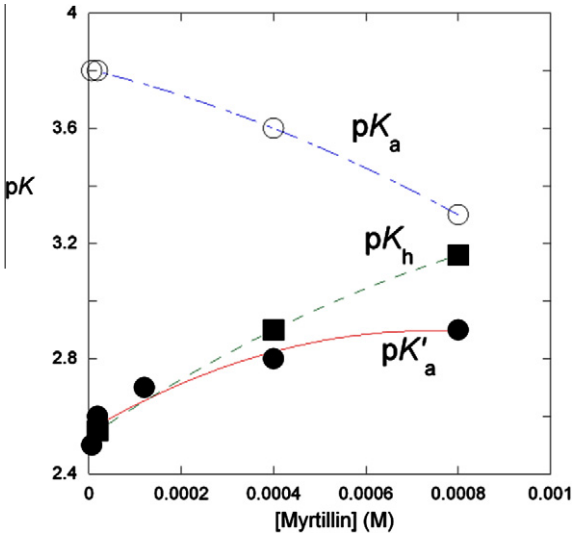

Fig. 6. Representation of the apparent equilibrium constants K_a, K_h and K'_a as a function of myrtillin concentration, with the respective trend lines.

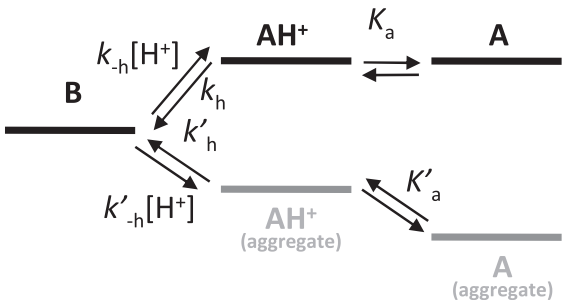

Scheme 4. Thermodynamic scheme showing the effect of the self-aggregation of flavylium cation and quinoidal base. The formation constant of the self-aggregate of quinoidal base is higher than the equivalent aggregate of flavylium cation.

and easy-to-stack structure. This point was confirmed by the value of the aggregation constants calculated for both species (see below Table 6) which resulted higher for **A**.

The rate and equilibrium constants of the hydration process for the concentrations 4×10^{-4} M (Supporting information) and 2×10^{-5} M are represented in Fig. 7.

As expected from Scheme 4, the hydration rate constant (k_h) decreases by increasing the anthocyanin concentration while the dehydration rate constant (k_{-h}) increases. The net result is the decreasing of the thermodynamic hydration constant K_h by increasing concentration. In the next section self-aggregation in anthocyanins and its effect on the respective rate and equilibrium constants are quantified.

3.2. Aggregation of flavylium cation

The effect of the self-association of the six anthocyanins in the flavylium form (pH = 1.0) was studied by ^{1}H NMR as a function of their respective concentration, Fig. 8 for myrtillin and Figs. S26–S30 of the Supporting information for the other anthocyanins. Inspection of these figures shows a high field shift of the resonance peaks as the concentration increases. Such type of effect was previously reported for oenin and other dyes and was attributed to the formation of aggregates (Houbiers et al., 1998). In Fig. 9 the chemical shifts of protons H4, H6 and H8 in ring A are represented as a function of the concentration. It is worth of note that at lower concentrations the chemical shift does not depend of the substitution pattern of the anthocyanins. This is an expected result if it is considered that the anthocyanins substituents are different only in ring B, having a negligible influence in protons H4, H6 and H8, if aggregation is not present. The observed chemical shifts can thus be interpreted as a result of the shielding of these protons upon the aggregation processes, an effect previously reported by different authors (Hoshino, 1992; Hoshino et al., 1982; Houbiers et al., 1998).

The observed shift to high field with concentration can be fitted with a simple model that assumes monomer–dimer fast equilibrium compared to the ^{1}H NMR time scale.

$$M + M \rightleftharpoons D \quad K_D = \frac{[D]}{[M]^2} \tag{13}$$

From the mass balance, where C_0 is the total concentration

$$C_0 = [M] + 2[D] \tag{14}$$

The mole fraction of the monomer and dimer can be obtained, respectively, by Eqs. (15) and (16)

$$\chi_M = \frac{-1 + \sqrt{1 + 8K_D C_0}}{4K_D C_0} \tag{15}$$

$$\chi_D = 1 - \chi_M \tag{16}$$

Fitting of the concentration dependent chemical shifts, as those reported in Fig. 8, can be achieved by means of Eq. (17)

$$\delta_{obs}(C_0) = \chi_M \delta_M + \chi_D \delta_D \tag{17}$$

δ_M and δ_D standing, respectively, for the chemical shifts of the monomer and dimer.

The global fittings, jointly employing the chemical shifts of protons H4, H6 and H8 are shown in Fig. 9 and the dimerization constants, together with monomer and dimer chemical shifts, which were used to fit the data, are summarized in Table 3.

In Table 4 the dimerization constants are presented according to the number of –OH and $-OCH_3$ substituents, evidencing the existence of a stronger aggregation by increasing the number of these substituents (Hoshino, 1992).

Formation of aggregates of order higher than two was suggested by other authors (Hoshino, 1991, 1992; Hoshino et al., 1980, 1981a,b, 1982; Houbiers et al., 1998). In this work good fittings have been obtained considering exclusively the monomer–dimer fast equilibrium. However indirect evidence for the formation of high order aggregates was achieved, see below.

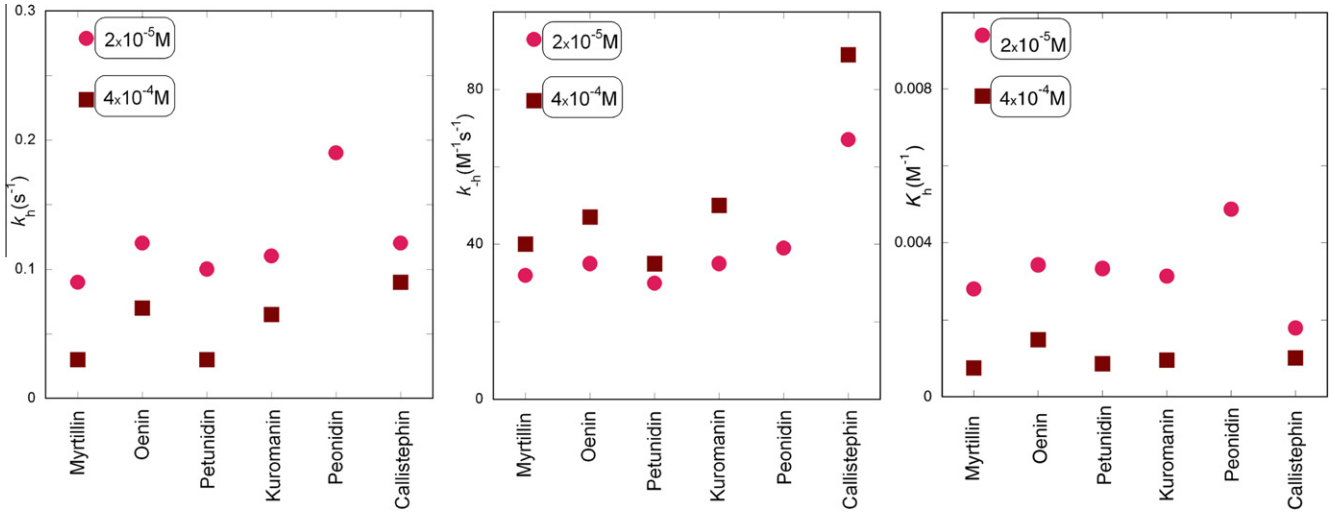

Fig. 7. Representation of the observed hydration constants, k_h, k_{-h} and K_h for the anthocyanin concentrations 2×10^{-5} M (●) and 4×10^{-4} M (■). The data at 4×10^{-4} M for 3-OGl-peonidin are not available due to precipitation in moderately acidic solutions.

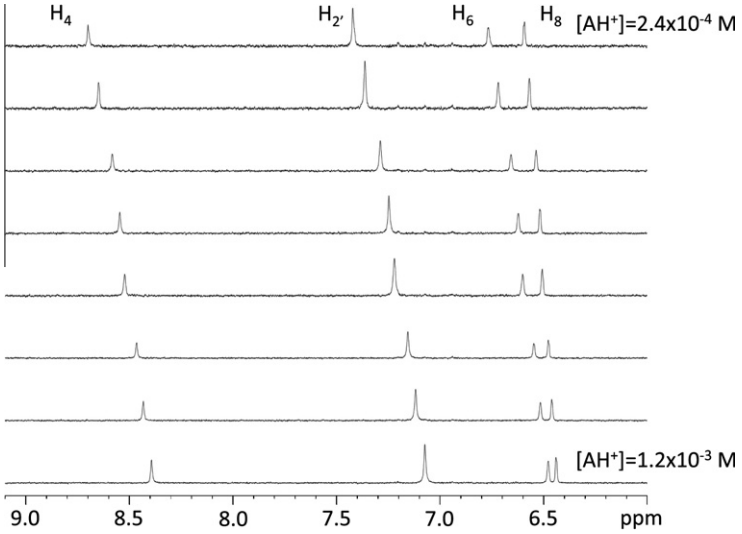

Fig. 8. ^{1}H NMR spectra of the compound myrtillin as a function of the concentration at pH = 1.0.

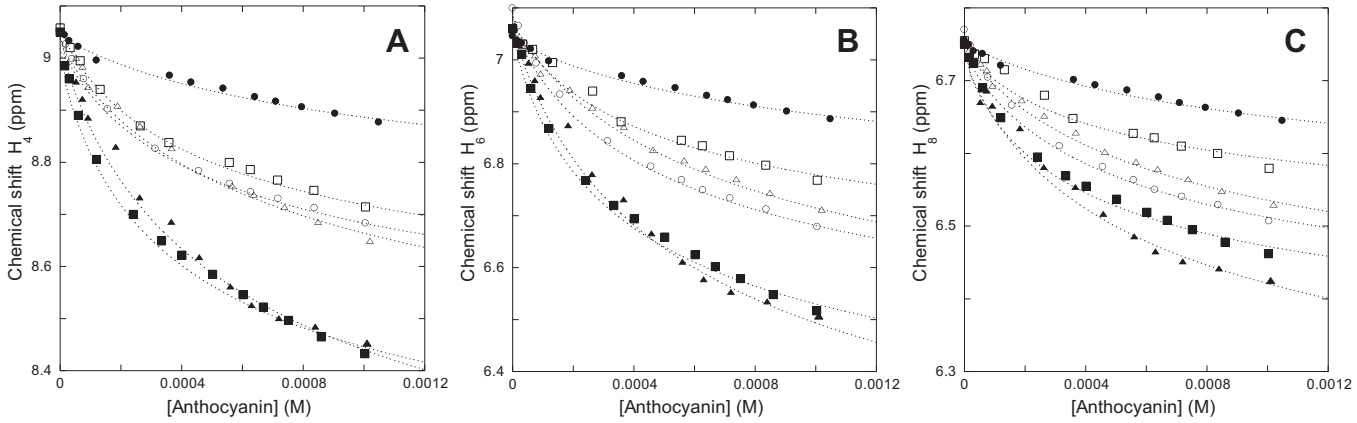

Fig. 9. Representation of the chemical shifts of protons, H_4 (A), H_6 (B) and H_8 (C) at pH = 1.0: callistephin (●), oenin (○), myrtillin (■), kuromanin (□), petunidin-3-glucoside (▲), peonidin-3-glucoside (△).

Table 3
Dimerization constants and chemical shifts obtained from fitting of the data reported in Fig. 9.

Anthocyanin	K_D (M^{-1})[a]	H4		H6		H8	
		δ_M (ppm)	δ_D (ppm)	δ_M (ppm)	δ_D (ppm)	δ_M (ppm)	δ_D (ppm)
Myrtillin	1240	9.05	7.99	7.05	6.09	6.76	6.22
Oenin	976	9.05	8.32	7.09*	6.27	6.76	6.27
Petunidin-3-OGl	900	9.05	7.78	7.05	5.85	6.76	6.07
Kuromanin	700	9.05	8.3	7.07*	6.37	6.76	6.36
Peonidin-3-OGl	661	9.05	8.16	7.05	6.22	6.76	6.25
Callistephin	404	9.05	8.58	7.05	6.61	6.76	6.45

[a] Estimated error 5%; δ_M – chemical shift of the monomer; δ_D – chemical shift of the dimer.
* Fitting is slightly better with these values than 7.05.

Table 4
Dimerization constants vs –OH and –OCH_3 substituents in the anthocyanin.

Anthocyanin	K_D (M^{-1})	OH	OCH_3
Myrtillin	1240	2	–
Oenin	976	–	2
3-OGl-Petunidin	900	1	1
Kuromanin	700	1	–
3-OGl-Peonidin	661	–	1
Callistephin	404	–	–

3.3. The isodesmic model

If aggregates of higher order are considered they will be accounted for by Eqs. (18)–(20)

$$M + M \rightleftarrows M_2 \quad c_2 = K_2 c_1^2 \tag{18}$$

$$M_2 + M \rightleftarrows M_3 \quad c_3 = K_3 c_2 = K_2 K_3 c_1^3 \tag{19}$$

$$M_{n-1} + M \rightleftarrows M_n \quad c_n = K_{n-1} c_{n-1} = K_2 K_3 \ldots K_n c_1^n \tag{20}$$

Scheme 5. Sketch showing the three types of environment of the aggregates; open discs-solvent, bars-anthocyanins.

where c_x is the concentration of the aggregate x: 1 – monomer, 2 – dimer etc.. . .; c_0 is the total concentration and K_x is the aggregation constant of the corresponding process.

In the isodesmic model it is assumed that all the K_n constants are equal i.e. $K_n = K$.

As shown in Supporting information the mole fraction distribution of the monomer and the aggregates is given by Eq. (21)

$$\frac{c_1}{c_0}+\frac{2Kc_1^2}{c_0}+\frac{3K^2c_1^3}{c_0}+\ldots+\frac{nK^{n-1}c_1^n}{c_0}=1 \tag{21}$$

with

$$c_0=\frac{c_1}{(1-c_1K)^2} \tag{22}$$

and

$$c_1=\frac{1+2Kc_0-\sqrt{1+4Kc_0}}{2K^2c_0} \tag{23}$$

The fitting of the experimental chemical shifts can be done considering three types of protons: (i) monomer type protons, surrounded by solvent in both sides (M), (ii) dimer type protons, molecule with one side exposed to solvent and the other side exposed to an analogous molecule (D), (iii) trimer type protons, molecule surrounded by the analogous molecules in both sides (T). Even the high order aggregates have only these three types of molecular interactions. A given proton in an aggregate containing n monomers, should present the average chemical shifts of two dimer type protons and $n-2$ trimer type protons, Scheme 5 (Dimicoli and Hélène, 1973).

The observed chemical shift can be written according to Eq. (24)

$$\delta_{obs}=\frac{c_1}{c_0}\delta_M+\frac{2Kc_1^2}{c_0}\delta_D+\frac{2K^2c_1^3}{c_0}\delta_D+\frac{K^2c_1^3}{c_0}\delta_T+\frac{2K^3c_1^4}{c_0}\delta_D+\frac{2K^3c_1^4}{c_0}\delta_T\ldots+\frac{2K^{n-1}c_1^n}{c_0}\delta_D+\frac{(n-2)K^{n-1}c_1^n}{c_0}\delta_T \tag{24}$$

Eq. (24) can be rearranged into Eq. (25). If n trends to infinity, Eq. (25) represents a infinite geometric series and its solution does not depend on n.

$$\delta_{obs}=\frac{c_1}{c_0}\delta_M+\left(1+Kc_1+K^2c_1^2\ldots+K^{n-3}c_1^{n-3}\right)\frac{2Kc_1^2}{c_0}\delta_D+\left(1+2Kc_1+\ldots(n-4)K^{n-3}c_1^{n-3}\right)\frac{K^2c_1^3}{c_0}\delta_T$$

$$\delta_{obs}=\frac{c_1}{c_0}\delta_M+\frac{2Kc_1^2}{(1-Kc_1)c_0}\delta_D+\frac{K^2c_1^3}{(1-Kc_1)^2c_0}\delta_T \tag{25}$$

The fitting of Eq. (25) can be achieved by adjusting K, δ_M, δ_D, and δ_T, Table 5.

The uncertainty of the data is high and different sets of chemical shifts differing slightly can be achieved. In the data reported in Table 5, $\delta_T = \delta_D - (\delta_M - \delta_D)$ which is a reasonable progression for the chemical shifts. Nevertheless, the results presented in Table 5 should be viewed as a predicted trend.

The aggregation phenomenon is also observed by UV–vis spectroscopy. The thermal equilibrated absorption spectra of Myrtillin as a function of its total concentration is reported in Fig. 10A.

In order to detect the variations on the shape of the absorption bands as a function of the anthocyanins concentration, the set of spectra presented in Fig. 10A was transformed into mole absorption coefficients, ε (M^{-1} cm^{-1}), dividing by the concentration and optical path, Fig. 10B. This figure shows, by increasing concentration, the split of the flavylium absorption band in two bands with maximum *ca.* 440 nm and 600 nm. This type of split suggests formation of aggregates exhibiting a shape between J and H (McRae and Kasha, 1958). The fitting was achieved considering a monomer–dimer equilibrium with a dimerization constant of 1260 M^{-1}, in good agreement with the data from ^{1}H NMR. The data is also compatible with the isodesmic model used to treat the ^{1}H NMR data.

The spectra from Fig. 10B were treated by *multires program* (Antonov and Petrov, 2002) and the following dimer parameters were calculated: $\alpha = 54°$ and $R = 5.0$ Å (see Scheme 6 and Supporting information).

3.4. Aggregation of the other species

The flavylium cation (**AH$^+$**) is dominant at very acidic pH values and the question is which kind of aggregates are formed at higher pH values and how they influence the kinetics and the thermodynamics of the network.

3.5. Simple aggregation model using monomer–dimer interactions

Evidences for self-aggregation of flavylium cations and quinoidal bases were reported above (see Fig. 6 and discussion about the effect of the concentration on K_a, K_h and K'_a). In previous work Hoshino and Goto (1990) reported the formation of dimers for the quinoidal base and ionized quinoidal base of Malvin. In this work the pH range (acidic to moderately acidic) prevents formation of

Table 5
Isodesmic constants and chemical shifts (ppm) obtained from the fitting of the data reported in Fig. 9 (and the equivalent for the other anthocyanins).

Anthocyanin	K_{isod} (M^{-1})[a]	H4			H6			H8		
		δ_M[1]	δ_D[1]	δ_T[1]	δ_M[1]	δ_D[1]	δ_T[1]	δ_M[1]	δ_D[1]	δ_T[1]
Myrtillin	2239	9.02	8.47	7.92	7.06	6.55	6.04	6.75	6.48	6.21
Oenin	1738	9.05	8.67	8.29	7.08	6.66	6.25	6.76	6.5	6.23
3-OGl-Petunidin	1349	9.04	8.34	7.64	7.08	6.4	5.72	6.74	6.37	6
Kuromanin	1259	9.05	8.65	8.26	7.07	6.72	6.37	6.76	6.55	6.35
3-OGl-Peonidin	871	9.04	8.5	7.97	7.06	6.59	6.11	6.75	6.45	6.15
Callistephin	525	9.04	8.76	8.47	7.04	6.78	6.51	6.75	6.57	6.39

[a] Estimated error 5%.
[1] ppm.

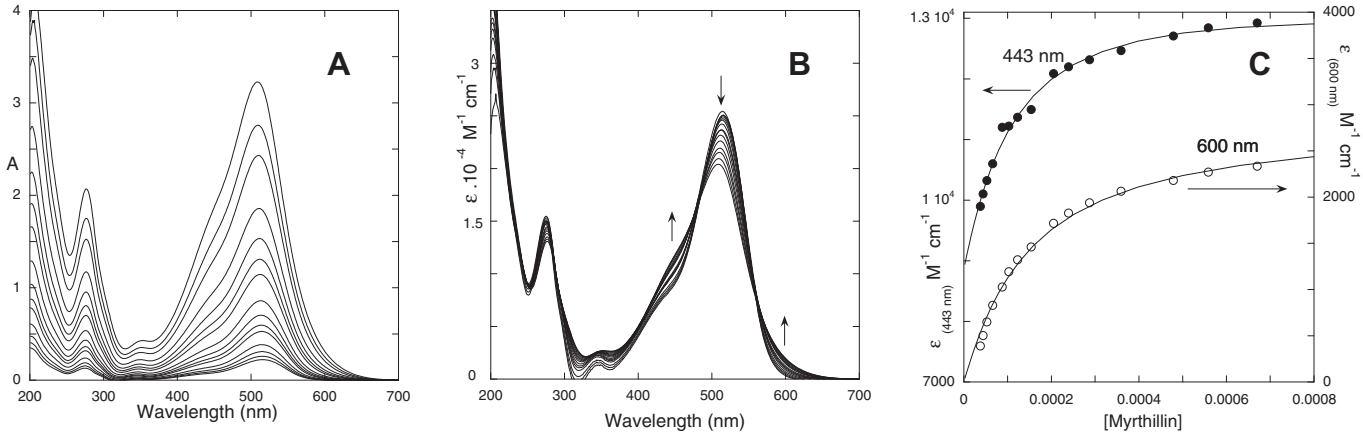

Fig. 10. (A) Absorption spectra of myrtillin as a function of the concentration: optical path 0.2 cm, in the concentration range 2.09×10^{-5} M < [myrtillin] < 6.2×10^{-4} M, pH = 1.0 (0.1 M HCl); (B) The spectra in B were normalized to observe the characteristic splitting of the absorption bands upon aggregation; (C) Concentration dependence of the absorption spectrum of myrtillin at 443 nm and 600 nm.

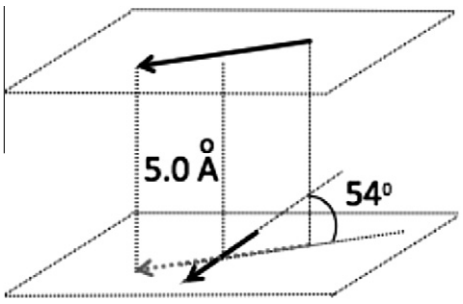

Scheme 6. Representation of the relative position of the transition dipole of myrtillin flavylium cations in a dimer.

ionized quinoidal bases and thus we limit the aggregation model to flavylium cation and quinoidal base Eqs. (26) and (27).

$$\mathbf{AH^+} + \mathbf{AH^+} \leftrightharpoons \mathbf{AH^+}\text{–}\mathbf{AH^+} \quad K_{\mathbf{DAH^+}} \tag{26}$$

$$\mathbf{A} + \mathbf{A} \leftrightharpoons \mathbf{A}\text{–}\mathbf{A} \quad K_{\mathbf{DA}} \tag{27}$$

The mixed dimers **AH⁺–Ct**, **AH⁺–A** and **A–Ct** were considered in a first version of the model but their contribution is not needed to achieve a good fitting. The **AH⁺–A** dimer, could in principle be formed from deprotonation of one **AH⁺** unit in the **AH⁺–AH⁺** dimer, whereas the deprotonation of the second **AH⁺** unit would give rise to the formation of the **A–A** dimer. However, we were not able to observe two deprotonation steps.

Considering the two self-dimers, the balance leads to

$$C_0 = [\mathbf{AH^+}] + [\mathbf{A}] + [\mathbf{B}] + [\mathbf{Cc}] + [\mathbf{Ct}] + 2[\mathbf{AH^+}\text{–}\mathbf{AH^+}] + 2[\mathbf{A}\text{–}\mathbf{A}] \tag{28}$$

Using the equilibrium constants all the species can be written as a function of [**AH⁺**]

$$2\left(K_{\mathbf{DAH^+}} + K_{\mathbf{DA}}\frac{K_a^2}{[H^+]^2}\right)[\mathbf{AH^+}]^2 + \left(1 + \frac{K'_a}{[H^+]}\right)[\mathbf{AH^+}] - C_0 = 0 \tag{29}$$

where K'_a was previously defined in Eq. (5). Resolution of Eq. (29) permits to obtain the pH dependent concentration of **AH⁺**.

In the ^{1}H NMR spectrum, the flavylium cation, the quinoidal base and respective dimers appear as a single peak due to their fast exchange in comparison with the ^{1}H NMR timescale, Eq. (30). The mole fraction of the other species are easily calculated from the respective equilibrium equations, Eqs. (31)–(33).

$$\chi_{\mathbf{AH^+}+\mathbf{A}+\mathbf{DAH^+}+\mathbf{DA}} = \frac{[\mathbf{AH^+}] + \frac{K_a}{[H^+]}[\mathbf{AH^+}] + 2\left(K_{\mathbf{DAH^+}} + K_{\mathbf{DA}}\frac{K_a^2}{[H^+]^2}\right)[\mathbf{AH^+}]^2}{C_0} \tag{30}$$

$$\chi_B = \frac{K_h}{[H^+]}\chi_{\mathbf{AH^+}} \tag{31}$$

$$\chi_{\mathbf{Cc}} = \frac{K_h K_t}{[H^+]}\chi_{\mathbf{AH^+}} \tag{32}$$

$$\chi_{\mathbf{Ct}} = \frac{K_h K_t K_i}{[H^+]}\chi_{\mathbf{AH^+}} \tag{33}$$

Fittings were made using the pH dependent mole fraction distribution of the species observed in the ^{1}H NMR experiments (see Fig. 5 for myrtillin), considering Eqs. (29)–(33), taking the values for K_h, K_i, and K_a (Table 1) and adjusting the dimerization constants, Table 6.

Table 6
Aggregation constants.

	log $K_{\mathbf{DAH^+}\,ag}$ [a]	log $K_{\mathbf{DA}}$ [a]
Myrtillin (M)		
0.0008	3.5	5.4
0.0004	3.4	5.0
2×10^{-5}*	3.35	-
Oenin (M)		
0.0008	3.4	5.4
0.0004	3.3	5.2
2×10^{-5}*	3.24	-
Petunidin (M)		
0.0008	3.3	5.3
0.0004	3.2	4.9
2×10^{-5}*	3.13	-
Kuromanin		
0.0008	3.2	5.3
0.0004	3.2	5.3
2×10^{-5}*	2.91	-
Callistephin		
0.0008	3.4	5.0
0.0004	3.2	5.0
2×10^{-5}*	2.72	-

[a] Estimated error 5%.
* pH = 1, from Table 3.

The data shown in Table 6 are one of the possible fitting solutions and the reported results should be viewed as a trend. In spite of the uncertainty of the data reported in Table 6 it is clear that the dimerization constants change with concentration. This is an indirect evidence for the formation of high order aggregates, and corroborates previous reports suggesting the formation of these species (Hoshino, 1991, 1992; Hoshino et al., 1980, 1981a,b, 1982; Houbiers et al., 1998).

4. Conclusions

The most surprising observation in this study is the relatively small influence of the anthocyanins substitution pattern into the thermodynamic and kinetics constants of the respective network of chemical reactions at low concentration. This was observed for the ^{1}H NMR chemical shifts of protons H4, H6 and H8, and is also observed when the equilibrium constants and the rate constants are compared: their differences are contained in a relatively small interval, see Table 1 and Table 3. However, the influence of the substitution pattern in these anthocyanins is clearly observed in the aggregation processes. Methoxy and hydroxy substituents favor the flavylium cation aggregation process suggesting for the hydrogen bonding a role in the aggregation mechanism. In spite of the good fitting of the ^{1}H NMR data with a simple monomer dimer model, for a fixed concentration, the recovered rate constants for the dimerization are not independent on the anthocyanin concentration, an indirect evidence for the formation of higher order aggregates. In the case of myrtillin, the compound where aggregation in the flavylium cation is stronger, the dipole moments of the two flavylium molecules in the dimer make an angle of 54° and are separated by 5 Å.

Acknowledgments

This work was supported by Fundação para a Ciência e Tecnologia, through National NMR Network, projects PTDC/QUI-QUI/117996/2010, SFRH/BPD/44230/2008 (YL), SFRH/BPD/44639/2008 (RG), SFRH/BPD/18214/2004 (VP), SFRH/BD/48226/2008 (AD).

Appendix A. Supplementary data

Supplementary data associated with this article can be found, in the online version, at http://dx.doi.org/10.1016/j.phytochem.2012.06.022.

References

Antonov, L., Petrov, V., 2002. Quantitative analysis of undefined mixtures – "Fishing net" algorithm. Anal. Bioanal. Chem. 374, 1312–1317.
Asen, S., Steward, R.N., Norris, K.H., 1972. Copigmentation of anthocyanins in plant-tissues and its effect on color. Phytochemistry 11, 1139–1144.
Asen, S., Steward, R.N., Norris, K.H., 1975. Anthocyanin, flavonol copigments and pH responsible for larkspur flower color. Phytochemistry 14, 2677–2682.
Bagchi, D., Bagchi, M., Stohs, S.J., Das, D.K., Ray, S.D., Kuszynski, C.A., Joshi, S.S., Pruess, H.G., 2000. Free radicals and grape seed proanthocyanidin extract: Importance in human health and disease prevention. Toxicology 148, 187–197.
Brouillard, R., 1982. In: Markakis, P. (Ed.), Anthocyanins as Food Colors. Academic Press, New York, pp. 1–40.
Brouillard, R., Delaporte, B., 1977. Chemistry of anthocyanins pigments. 2. Kinetic and thermodynamic study of proton transfer, hydration and tautomerization reactions of malvidin-3-glucoside. J. Am. Chem. Soc. 99, 8461–8468.
Brouillard, R., Lang, J., 1990. The hemiacetal-cis-chalcone equilibrium of malvin, a natural anthocyanin. Can. J. Chem. 68, 755–761.
Brouillard, R., Delaporte, B., Dubois, J.-E., 1978. Chemistry of anthocyanin pigments. 3. Relaxation amplitudes in pH-jumps experiments. J. Am. Chem. Soc. 100, 6202–6205.
Bülow, C., Wagner, H., 1901. Ueber derivate des 1,4-benzopyranols, der muttersubstanz einer neuen klasse von farbstoffen. II. Ber. Dtsch. Chem. Ges. 34, 1782–1804.
Castañeda-Ovando, A., Pacheco-Hernandez, M.D., Paez-Hernandez, M.E., Rodriguez, J.A., Galan-Vidal, C.A., 2009. Chemical studies of anthocyanins: A review. Food Chem. 113, 859–871.
Dangles, O., Saito, N., Brouillard, R., 1993. Kinetic and thermodynamic control of flavylium hydration in pelargonidin cinnamic acid complexation-origin of the extraordinary flower color diversity of pharbitis-nil. J. Am. Chem. Soc. 115, 3125–3132.
Dimicoli, J.-L., Hélène, C., 1973. Complex-formation between purine and indole-derivatives in aqueous-solutions-proton magnetic-resonance studies. J. Am. Chem. Soc. 95, 1036–1044.
Figueiredo, P., Lima, J.C., Santos, H., Vigand, M.-C., Brouillard, R., Maçanita, A.L., Pina, F., 1994. Photochromism of the synthetic 4′,7-dihydroxyflavylium chloride. J. Am. Chem. Soc. 116, 1249–1254.
Glasoe, P.K., Long, F.A., 1960. Use of glass electrodes to measure acidities in deuterium oxide. J. Phys. Chem. 64, 188–190.
Goto, T., Kondo, T., 1991. Structure and molecular stacking of anthocyanins-flower color variation. Angew. Chem. Int. Ed. Engl. 30, 17–33.
Hoshino, T., 1991. Anthocyanin self-aggregates. 6. An approximation estimate of self-association constants and the self stacking of malvin quinonoidal bases studied by H-1-NMR. Phytochemistry 30, 2049–2055.
Hoshino, T., 1992. Self-association of flavylium cations of anthocyanidin-3,5-diglucosides by circular dichroism and ^{1}H NMR. Phytochemistry 31, 647–653.
Hoshino, T., Goto, T., 1990. Effects of pH and concentration on the self-association of malvidin quinonoidal base – Electronic and circular dichroic studies. Tetrahedron Lett. 31, 1593–1596.
Hoshino, T., Matsumoto, U., Goto, T., 1980. Evidence for self-association of anthocyanins. 1. Circular dichroism of cyanin anhydrobase. Tetrahedron Lett. 21, 1751–1754.
Hoshino, T., Matsumoto, U., Harada, N., Goto, T., 1981a. Chiral excitation couple stacking of anthocyanins. Interpretation of the origin of anomalous CD induced by anthocyanin association. Tetrahedron Lett. 22, 3621–3624.
Hoshino, T., Matsumoto, U., Goto, T., 1981b. Evidence for self-association of anthocyanins. 2. Self-association of some anthocyanins in neutral aqueous-solution. Phytochemistry 120, 1971–1976.
Hoshino, T., Matsumoto, U., Goto, T., 1982. Evidence for self-association of anthocyanins. 4. PMR spectroscopic evidence for the vertical stacking of anthocyanin molecules. Tetrahedron Lett. 23, 433–436.
Houbiers, C., Lima, J.C., Maçanita, A.L., Santos, H., 1998. Color stabilization of malvidin 3-glucoside: Self-aggregation of the flavylium cation and copigmentation with the Z-chalcone form. J. Phys. Chem. B 102, 3578–3585.
Kalt, W., Forney, C.F., Martin, A., Prior, R.L., 2001. Horticultural factors affecting antioxidant capacity of blueberries and other small fruit. J. Agric. Food Chem. 49, 170–176.
Kondo, T., Yoshida, K., Nakagawa, K.A., Kawai, T., Tamura, H., Goto, T., 1992. Structural basis of blue color development in flower petals from *Commelina communis*. Nature 358, 515–518.
Kondo, T., Oyama, K.-I., Yoshida, K., 2001. Chiral molecular recognition on formation of a metalloanthocyanin: A supramolecular metal complex pigment from blue flowers of Salvia paten. Angew. Chem. Int. Ed. Engl. 40, 894–897.
Mateus, N., Freitas, V., 2009. Anthocyanins as food colorants. In: Gould, K., Davies, K.M., Winefield, C. (Eds.), Anthocyanins-Biosynthesis Functions and Applications. Springer, pp. 283–304.
McClelland, R.A., Gedge, S., 1980. Hydration of the flavylium ion. J. Am. Chem. Soc. 102, 5838–5848.
McClelland, R.A., McGall, G.H., 1982. Hydration of the flavylium ion. 2. The 4′-hydroxyflavylium. J. Org. Chem. 47, 3730–3736.
McRae, E.G., Kasha, M., 1958. Enhancement of phosphorescence ability upon aggregation of dye molecules. J. Chem. Phys. 28, 721–722.
Pina, F., 1998. Photochromism of the synthetic 4′-7-dihydroxyflavylium chloride. J. Chem. Soc. Faraday Trans. 94, 2109–2116. Correction in Scheme 1. The Ct and Cc structures should, exchange, 1998, 94, 3781–3781.
Pina, F., Melo, M.J., Laia, C.A.T., Parola, A.J., Lima, J.C., 2012. Chemistry and applications of flavylium compounds: A handful of colours. Chem. Soc. Rev. 41, 869–908.
Popov, K., Rönkkömäki, H., Lajunen, L.H.J., 2006. Guidelines for NMR measurements for determination of high and low p*K*(a) values. Pure Appl. Chem. 78, 663–675.
Shaka, A.J., Hwang, T.-L., 1995. Water suppression that works-excitation sculpting using arbitrary wave-forms and pulsed-field gradients. J. Magn. Reson. A 112, 275–279.
Yoshida, K., Kondo, T., Okazaki, Y., Katou, K., 1995. Cause of blue petal color. Nature 373, 291.
Yoshida, K., Mori, M., Kondo, T., 2009. Blue flower color development by anthocyanins: From chemical structure to cell physiology. Nat. Prod. Rep. 26, 884–915.